Research Article | Vol. 28, No. 11 / 25 May 2020 / Optics Express 16352

Optics EXPRESS

Motion-free TSOM using a deformable mirror

JUN HO LEE,[1,*] BYEONG GEON YOU,[1] SHIN-WOONG PARK,[2] AND HWI KIM[2]

[1] *Department of Optical Engineering, Kongju National University, 1223-24 Cheonan-daero, Seobuk-gu, Cheonan 31080, South Korea*
[2] *ICT Convergence Technology for Health & Safety, Korea University, 2511 Sejong-ro, Sejong 30019, South Korea*
[*] *jhlsat@kongju.ac.kr*

Abstract: Through-focus scanning optical microscopy (TSOM) is a model-based optical metrology method that involves the scanning of a target through the focus of an optical microscope. Unlike a conventional optical microscope that directly extracts the diffraction-limited optical information from a single in-focus image, the TSOM method extracts nanometer scale sensitive information by matching the target TSOM data/image to reference TSOM data/images that are either experimentally or computationally collected. Therefore, the sensitivity and accuracy of the TSOM method strongly depends on the similarities between the conditions in which the target and reference TSOM images are taken or simulated, especially the lateral instability during through-focus scanning. As a remedy to the lateral instability, we proposed the application of adaptive optics to the through-focus scanning operation and initially developed a closed-loop system with a tip/tilt mirror and a Shack-Hartmann sensor, with which we were able to keep the plane position within peak-to-valley (PV) 33 nm. We then further developed a motion-free TSOM tool reducing the instability down to practically zero by the replacement of the tip/tilt mirror with a deformable mirror that performs through-focus scanning by deforming its mirror surface. The motion-free TSOM tool with a × 50 (NA 0.55) objective lens could provide a scanning range of up to ± 25 µm with a minimum step of 25 nm at a maximum update rate of 4 kHz. The tool was demonstrated to have a recognition accuracy of < 4 nm for critical dimension (CD) values in the range of 60 ~ 120 nm with a reference TSOM image library generated by a Fourier modal method matching various observations conditions.

1. Introduction

Through-focus scanning optical microscopy (TSOM) is an optical model-based metrology method that was developed to overcome the classical resolution limit due to diffraction in optical microscopy [1–3]. This bright-field microscopy technique uses an ordinary optical reflection microscope but produces nanometer dimensional measurement sensitivity [4–9]. In comparison to a conventional bright-field microscope, which directly extracts the diffraction-limited optical information from a single in-focus image, TSOM indirectly extracts nanometer scale sensitive information by analyzing stacked through-focus (TF) images as a whole (TSOM data cube) or a cross-sectional image along the scanning direction, which is referred to as a TSOM image. The TSOM data analysis typically includes library-matching [4–9] or machine-learning methods [10,11]. Both methods require reference TSOM data/images that are either experimentally or computationally collected. Therefore, the sensitivity and accuracy of the TSOM method strongly depends on the similarities between the conditions in which the target and reference TSOM data/images are acquired or simulated. Figure 1 provides a schematic diagram of the TSOM process describing four major steps: 1) through-focus scanning along the optical axis, 2) image acquisition at multiple through-focus positions during the scanning process, 3) TSOM data cube/image generation, and 4) TSOM data processing.

#394939 https://doi.org/10.1364/OE.394939
Journal © 2020 Received 10 Apr 2020; revised 8 May 2020; accepted 9 May 2020; published 14 May 2020

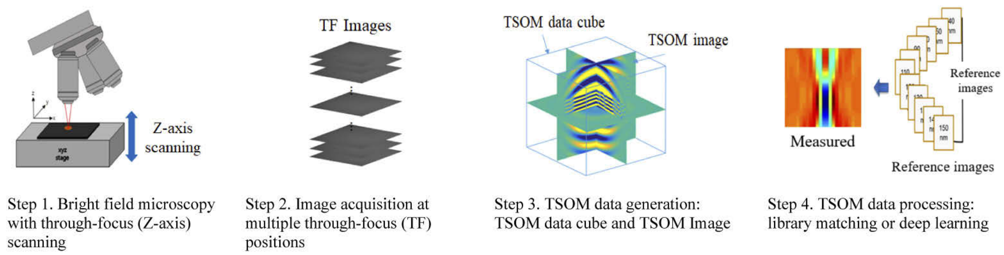

Fig. 1. Schematic diagram of the TSOM process

It should be emphasized again that TSOM is a nanodetection technique but does not provide real improved resolving power such as fluorescent stimulated emission depletion microscopy (STED) [12]. The nanometer sensitivity is obtained with great care paid in optimizing the image acquisition conditions such as averaging, noise reduction, and calibration, and in normalizing the images so that they can be compared with each other or with a library of images from a reference library [3,13–14]. In particular, major efforts have been focused on mitigation of the dissimilarity in the through-focus scanning and illumination conditions in which the target and reference TSOM images are taken or simulated [15–23].

Regarding the mitigation efforts for the instability issue, several approaches have been proposed: 1) a z-axis scanning-free strategy utilizing the residual chromatic aberration of an objective lens [15,16]; 2) temporal averaging by the exposure time increment [17]; 3) instability correction with Fourier transform [18,19]; and 4) active compensation by the use of adaptive optics technology [20–22]. The first approach requires precise knowledge of the residual chromatic aberration, which is not typically provided and it prohibits the use of monochromatic light sources such as lasers desired for high volume metrology and inspection applications [24]. The second approach averages out the random position instability by increasing the exposure time of the camera, which sacrifices the efficacy or the throughput. In addition, the slow lateral movement such as drift cannot be removed out even after the temporal averaging. The third approach, i.e. lateral movement correction using Fourier transform, effectively decreases the lateral movement of the pattern image due to the optical and mechanical noise, simultaneously. But this approach requires precise knowledge of the target structure and material properties and the increased TSOM data processing time. The use of adaptive optics [25,26] was initially proposed to compensate the lateral jitter motion with a tip/tilt mirror close-looped with a Shack-Hartmann wavefront sensor in the imaging path of the microscope [20–22]. However, due to the limited angular resolution of the Shack-Hartmann sensor, the lateral position error is small but still non-zero, i.e. 33 nm in peak-to-valley (PV) value [22].

We here propose further improvement from the tip/tilt compensated TSOM, i.e. a motion-free TSOM. The motion-free TSOM reduces the instability down to practically zero by replacing the tip/tilt mirror with a deformable mirror which performs through-focus scanning by deforming its mirror surface.

2. Understanding of through-focus scanning process

2.1. Optical understanding of through-focus scanning

Figure 2 shows a schematic diagram of an infinite-conjugate microscope consisting of an objective lens, a tube lens, and a phase modulator located at the Fourier plane of the microscope, which is a deformable mirror in our study. In terms of geometrical optics, an object plane at the focus of the objective lens is conjugated to the image plane located at the focus of the tube lens with

Optics EXPRESS

lateral magnification M and longitudinal magnification M_z as follows:

$$M = \frac{\Delta x_i}{\Delta x_0} = \frac{\Delta y_i}{\Delta y_0} = -\frac{f_T}{f_0}, \tag{1}$$

$$M_z = \frac{\Delta z_i}{\Delta z_0} = -\left(\frac{f_T}{f_0}\right)^2 = -M^2. \tag{2}$$

f_0 and f_T are the focal lengths of the objective and tube lens. (x_0, y_0, z_0) and (x_i, y_i, z_i) are the coordinate systems of the object and image space with the origins at each focus, respectively.

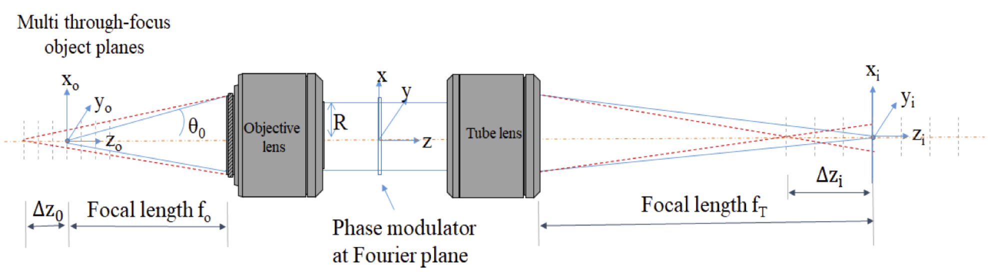

Fig. 2. Schematic diagram of an infinite-conjugate microscopy

When the object plane is shifted along the optical axis by an amount ε_z, the conjugated image plane is accordingly shifted along the optical axis by an amount $-M^2\ \varepsilon_z$. Without the corresponding shift of either the object plane or image plane, the imaging is referred to as defocused. In terms of wave optics, the wavefront aberration $W(x, y)$ of the defocused imaging is given as

$$W(x, y) = -\frac{1}{2}(NA_o)^2\,(\varepsilon_z)\left(\frac{x^2+y^2}{R^2}\right) + W_{residual}\,(x, y) + W_{DM}\ (x, y)\,. \tag{3}$$

where:

(x,y) = coordinate in the Fourier plane

NA_o = numerical aperture (NA) of the objective lens

ε_z = amount of defocus in the object plane

R = maximum beam radius at the Fourier plane of the objective lens

$W_{residual}$ = residual aberration of the objective lens

W_{DM} = wavefront deformation by a phase modulator such as a deformable mirror

Therefore, the through-focus scanning can be done by changing either the object or image distances or by generating equivalent optical aberrations by chromatic sweeping or active phase modulation. Attotta thoroughly reviewed over 15 types of through-focus image acquisition methods potentially suitable for TSOM [27]: scanning the sample stage along the focus axis, scanning the objective lens along the focus axis, scanning the image plane along the focus axis, multifocal plane microscopy, wavelength scanning method, flexible-membrane liquid lens, liquid-tunable lens, adaptive optics, multifocus microscopy, aperture-scanning Fourier ptychography, confocal microscopy, light sheet microscopy, light field microscopy, phase retrieval techniques, and digital holography microscopy. Among the reported methods, sample stage scanning is most widely used in the TSOM studies by adopting a manual or motorized z-axis stage [2,4–11,13,14,16,19,23].

Optics EXPRESS

2.2. Numerical simulation of through-focus scanning

Many studies numerically simulated the through-focus scanning process by iterative calculation of the light field with movement of the target [2,4–9,11–17]. Recently, a Fourier modal method (FMM) was proposed to improve the computational efficiency by applying a once-solved scattering matrix in the frequency domain to obtain field distributions at any z-position [18], which was used for building up reference TSOM images in this study.

2.3. Necessity of stable through-focus scanning mechanism

The use of the mechanical scanning inevitably incurs positional ambiguity and instability, mostly in the lateral direction across the through-focus scanning direction. First, sub-pixel position ambiguity naturally exists due to the use of a finite sized detector which fundamentally limits the accuracy of the TSOM method. Second, it is very costly to remove relevant random jitter and slow drift during the z-axis stage operation, especially when dealing with targets of nanometer feature size. It was reported that the slow-drift or tilt in the TSOM image can also occur due to non-uniform angular illumination asymmetry (ANILAS) across the field-of-view [28,29]. Figure 3 shows conceptual TSOM image stacks with the lateral positional ambiguity and instability and corresponding exemplary simulated TSOM images.

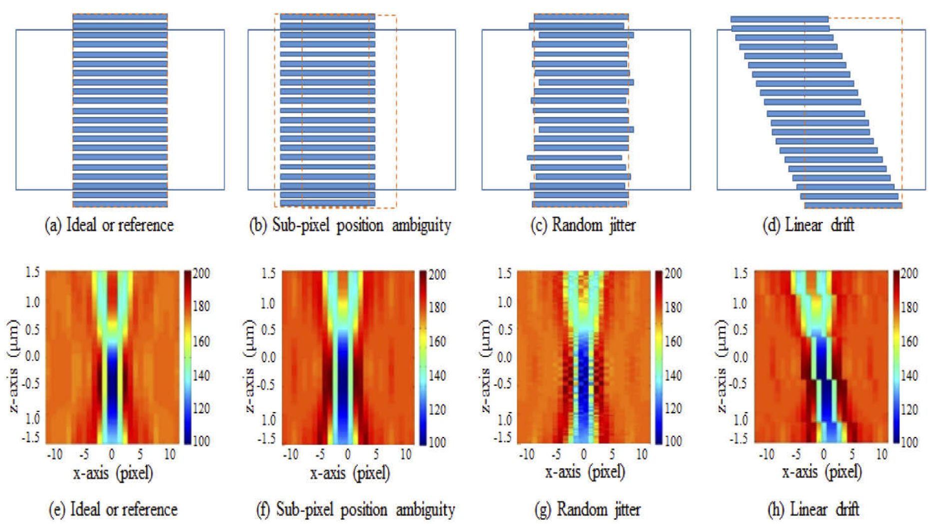

Fig. 3. TSOM image stacks with the lateral positional ambiguity and instability: (a)-(d) conceptual and (e)-(h) exemplary simulated TSOM images

A quantitative analysis was studied to investigate the effect of the lateral position errors over the TSOM method for critical dimension (CD) measurement on a 60 nm single line fin pattern based on the mean square deference (MSD) as given by

$$\mathrm{MSD} = \frac{1}{\mathrm{N}} \sum\nolimits_{\mathrm{i}=1}^{\mathrm{N}} \left(\mathrm{TSOM}^{(\mathrm{i})}{}_{\mathrm{Target}} - \mathrm{TSOM}^{(\mathrm{i})}{}_{\mathrm{Reference}}\right)^2. \tag{4}$$

We computationally built ideal images of single line fin patterns of linewidth 55 ~ 65 nm with 1 nm step without any positional errors and the target TSOM images by adding individual positional errors with different magnitudes to the ideal TSOM image of 60 nm with single fin: 1) sub-pixel ambiguity up to 30 nm, 2) random jitter with Gaussian distribution up to 30 nm, and 3) linear drift with a slope angle up to 0.5°. The detailed simulation conditions are tabulated in Table 1.

Figure 4 shows the mean square differences (MSD) variations due to CD change and various positional errors of a 60 nm linewidth single line fin pattern. The MSD value of 31.2×10^{-4}

corresponds to the 10% CD difference, i.e. 6 nm. For securing 10% CD measurement accuracy, the sub-pixel position ambiguity, random jitter, and liner drift should be smaller than 15 nm, 12 nm, and 0.4 degree, respectively. Therefore, it is obviously necessary to reduce the positional errors for achieving nm measurement sensitivity in the TSOM method.

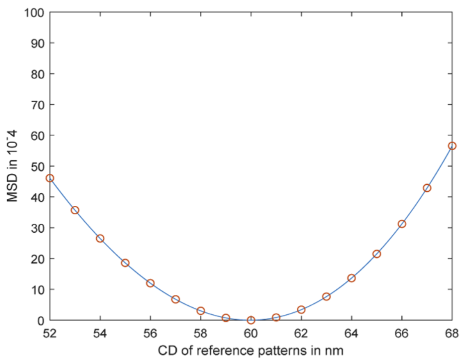

(a) CD changes

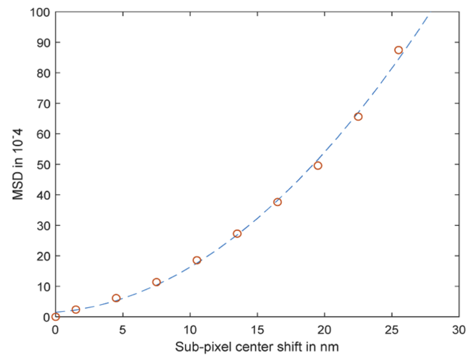

(b) Sub-pixel position ambiguity

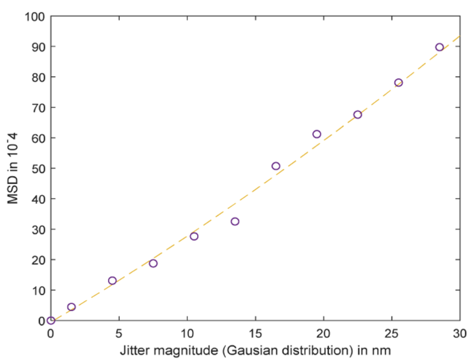

(c) Random jitter

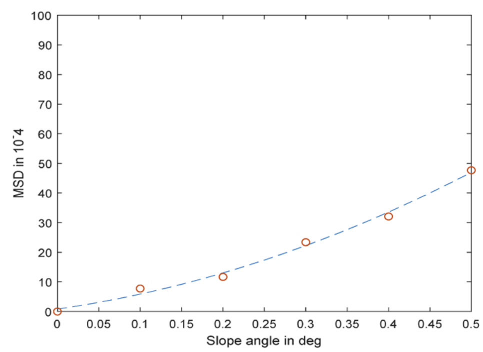

(d) Linear drift

Fig. 4. MSD variations due to (a) CD change and (b)-(d) individual positional errors of 60 nm linewidth single line fin pattern.

Table 1. TSOM simulation conditions for investigating the lateral instability and ambiguity.

	Items	Values	Note
Imaging conditions	Wavelength	600 nm	
	Illumination NA	0.3	
	Collection NA	0.55	
	Objective magnification	× 50	Relay lens magnification × 1
	Sampling distance on wafer	150 nm	Pixel scale conversion on the images
	Detector pitch	7.5 µm	
	Viewing length (x-axis)	3 µm	20 pixels
Through-focus (Z axis) scanning	Range (z-axis)	2 µm	- 1.0 ~ + 1.0 µm
	No of steps	101	Δ = 20 nm

Optics EXPRESS

3. Implementation

3.1. Adaptive optics supported TSOM

Adaptive optics is an optical technology that removes the wavefront distortion introduced by a turbulent medium by introducing a controllable counter wavefront distortion that both spatially and temporally follows that of the disturbance [25,30]. The use of adaptive optics technology was proposed to actively compensate the lateral instability via two approaches [20–22]. The first approach uses a simple tip/tilt mirror to compensate any optical-axis instability while moving the wafer stage. The second approach uses a deformable mirror to optically perform the through-focus scanning without any mechanical movement. Figure 5 presents schematic diagrams of the two approaches.

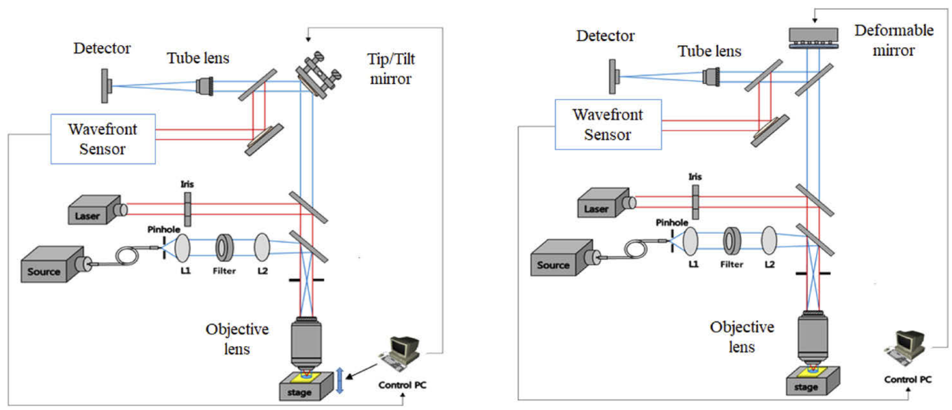

(a) Tip/tilt compensated TSOM with through-focus scanning provided by a motorized z-axis stage

(b) Motion-free TSOM with through-focus scanning provided by a deformable mirror

Fig. 5. Schematic diagram of the adaptive optics supported TSOM

3.2. Experience with a tip/tilt correction TSOM implementation

The first approach was implemented on an optical bench with commercial off-the-shelf components. The technical details of the implementation are tabulated in Table 2. The motorized z-axis stage experienced center beam movement of 4.1 µm over the 3.0 µm z-axis scanning, as seen in Fig. 6(a). With the help of the active tip/tilt compensation, the beam movement was dramatically reduced down to 33 nm in PV (peak-valley), as presented in Fig. 6(b). However, considering the results of section 2.3, further reduction of the positional error is still desired.

Table 2. Main parameters of a tip/tilt corrected TSOM implementation.

Component	Parameter	Value	Note
Motorized Z-stage	Min achievable incremental movement	0.1 µm	Thorlab (MT1/M-Z8)
Tip/tilt mirror	Angular resolution	6 arcsec	Thorlab (KS1-Z8)
Shack-Hartmann sensor	Wavefront Sensitivity	λ /15 RMS at 633 nm	Thorlab (WFS150-7AR)

Optics EXPRESS

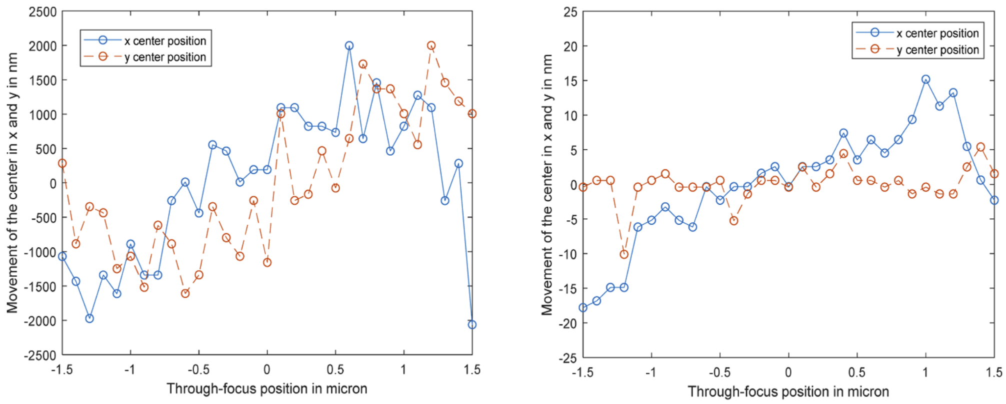

(a) Beam movement without tip/tilt correction

(b) Beam movement with tip/tilt correction

Fig. 6. Beam center movement of a tip/tilt corrected TSOM during the through-focus scanning process without and with tip/tilt correction

3.3. Motion-free TSOM with a deformable mirror

There are several types of deformable mirrors (DMs) including stacked array, bimorph, voice-coil actuator, micro electro-mechanical system (MEMS), and optically addressed DMs [30,31]. Among them, a bimorph DM is chosen in our study since it provides excellent correction or formation of most common optical aberrations, especially focus [32,33].

The wavefront deformation of the deformable mirrors can be controlled via either zonal or modal control approaches. In the modal control approach, each control channel corresponds to one optical mode, which is often a Zernike polynomial. The wavefront deformation $W_{DM}\ (x, y)$ is then expressed by

$$W_{DM}\ (x, y) = \sum_i b_i Z_i\,(x, y) \tag{5}$$

where $Z_i(x, y)$ is the i$^{\text{th}}$ Zernike polynomial and b_i the corresponding control signal. Defocus corresponds to the 4$^{\text{th}}$ Zernike polynomial $Z_4(x, y)$, as given below [34]:

$$Z_4\,(x, y) = \sqrt{3}\left(2\left(\frac{x^2 + y^2}{R^2}\right) - 1\right). \tag{6}$$

Therefore, the target movement (ε_z) along the optical axis can be optically modulated by equivalent wavefront deformations with the control signal b_4 or the peak-to-valley (PV) physical stroke S of the DM at the DM maximum aperture R_{max}, given as

$$b_4 = -\frac{1}{4\sqrt{3}}(NA_0)^2 \varepsilon_z. \tag{7}$$

$$S = \frac{1}{4}(NA_0)^2\left(\frac{R_{max}}{R}\right)^2 \varepsilon_z \tag{8}$$

Figure 7 shows a motion-free TSOM tool developed with the technical details in Table 3. As expected from Eq. (8), the tool could provide a through-focus range of ± 25 µm with a 25 nm step for a × 50 (NA 0.55) objective lens. The illumination NA and spectrum could be simply changed by changing the aperture and spectral filter in the illumination path, marked as ⑧ in Fig. 7.

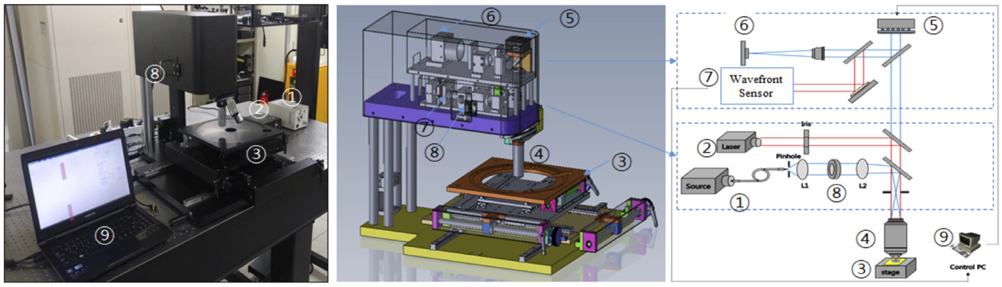

(a) Picture of a developed model b) 3D model c) Optical layout

Fig. 7. Developed motion-free TSOM tool: ① light source ② He-Ne laser ③ z-axis stage ④ objective lens ⑤deformable mirror ⑥ imaging detector ⑦ Shack-Hartmann wavefront sensor ⑧ aperture & spectral filter ⑨ control PC

Table 3. Main parameters of a motion-free TSOM implementation.

Component	Parameter	Value	Note
Objective lens	Magnification	× 50 (NA 0.55)	Switchable with × 100 (NA 0.7)
Light source	Spectrum	600 nm (10 nm FWHM)	Changeable with an aperture and band-pass filter
	Numerical aperture	0.3	
Deformable mirror	Pupil diameter	Ø 10.0 mm	Thorlab (DMP40)
	Defocus stroke	± 6.5 µm	PV at Ø 10.0 mm
Shack-Hartmann sensor	Wavefront Sensitivity	λ /15rms	Thorlab (WFS150-7AR)

3.4. Experiments with single line fin patterns

The sub-nanometer scale sensitivity of the motion-free TSOM tool was tested with four single line fin patterns having design width 60, 80, 100, and 120 nm with a height of 50 nm, which were measured to have CDs of 55.2, 78.9, 94.7, and 110.4 nm, respectively, by a scanning electron microscope (SEM), as shown in Fig. 8. Figure 9 shows the experimentally measured and corresponding simulated TSOM images of the four single line fin patterns. Each measured TSOM image was compared with reference TSOM images featuring sub-nanoscale linewidth variations in terms of the MSD. The linewidth (CD) could be estimated at the minimum point of the MSD under a reliable tolerance level of 0.1 nm [18]. The estimated line widths were all within 4 nm from the SEM measured values, as listed in Table 4.

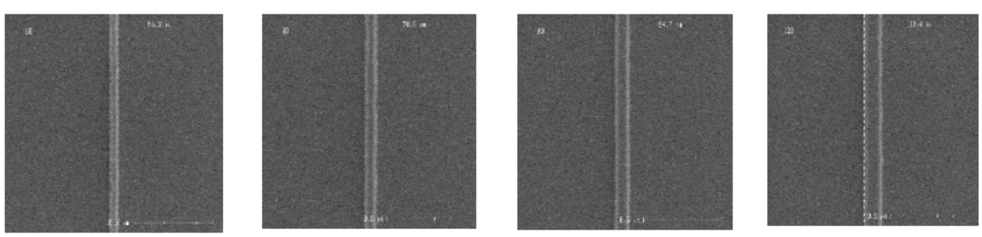

(a) 60 nm line pattern (CD = 55.2 nm) (b) 80 nm line pattern (CD = 78.9 nm) (c) 100 nm line pattern (CD = 94.7 nm) (c) 120 nm line pattern (CD = 110.4 nm)

Fig. 8. SEM images of the manufactured four single line fin patterns

Optics EXPRESS

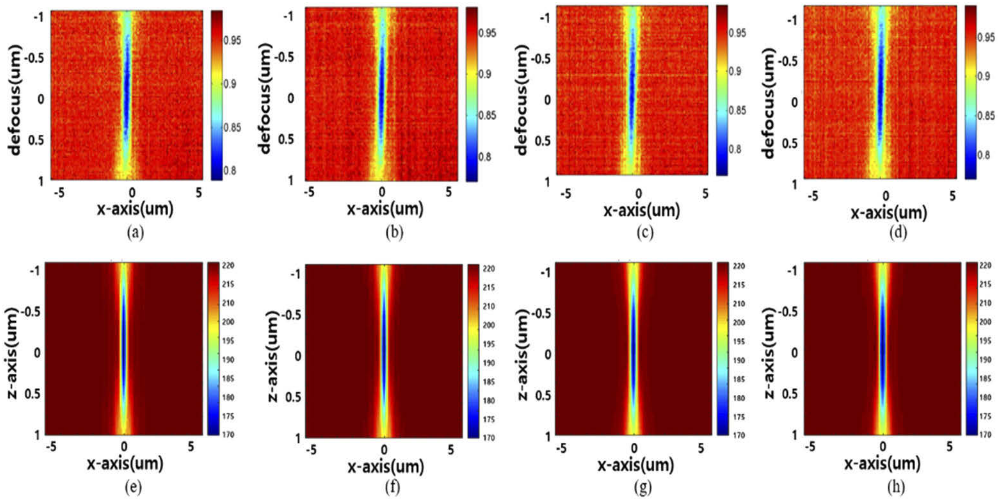

Fig. 9. TSOM images experimentally obtained by (a)-(d) the motion-free TSOM tool and numerically by (e)-(h) the Fourier Modal Method for the single fin patterns having width of 55.2, 78.9, 94.7, and 110.4 nm

Table 4. CD values of the four single line fin patterns in nm.

Design	SEM	TSOM	Difference
60	55.2	57.5	2.3
80	78.9	79.0	0.1
100	94.7	97.2	2.5
120	110.4	113.7	3.3

4. Conclusion

TSOM is a nanodetection technique that overcomes the resolution limit but the nanometer sensitivity only is obtained with great care paid in optimizing the image acquisition conditions and minimizing the dissimilarity in the through-focus scanning and illumination conditions in which the target and reference TSOM images are taken or simulated. Adaptive optics techniques were introduced to stabilize the through-focus scanning process. The first implementation with a tip/tilt mirror successfully reduced the PV lateral position error from 4 µm to 33 nm. However, it was necessary to further reduce the residual to a few nanometers. A motion-free TSOM by the use of a deformable mirror (DM) was then proposed. A motion-free TSOM tool with a bimorph mirror was developed and it could provide a through-focus range of ± 25 µm with a 25 nm increment for a ×50 (NA 0.55) objective lens. We demonstrated that the motion-free TSOM tool estimated the critical dimension (CD) values of single line fin patterns in the range of 60 ~ 120 nm with accuracy of < 4 nm based on the minimum MSD approach.

Funding

Ministry of Trade, Industry and Energy (10048720).

Disclosures

The authors declare no conflicts of interest.

Optics EXPRESS

References

1. Y. Ku, A. Liu, and N. Smith, "Through-focus technique for nano-scale grating pitch and linewidth analysis," Opt. Express **13**(18), 6699–6708 (2005).
2. R. Attota, T. A. Germer, and R. M. Silver, "Through-focus scanning-optical-microscope imaging method for nanoscale dimensional analysis," Opt. Lett. **33**(17), 1990–1992 (2008).
3. P. C. Montgomery, A. Leong-Hoi, F. Anstotz, D. Mitev, L. Pramatarova, and O. Haeberlé, "From superresolution to nanodetection: overview of far field optical nanoscopy techniques for nanostructures," J. Phys.: Conf. Ser. **682**, 012010 (2016).
4. R. Attota, R. Silver, and R. Dixson, "Linewidth measurement technique using through-focus optical images," Appl. Opt. **47**(4), 495–503 (2008).
5. R. Attota, R. Silver, and B. M. Barnes, "Optical through-focus technique that differentiates small changes in line width, line height, and sidewall angle for CD, overlay, and defect metrology applications," Proc. SPIE **6922**, 69220E (2008).
6. R. Attota, M. Stocker, R. Silver, A. Heckert, H. Zhou, R. Kasica, L. Chen, R. Dixson, G. Orji, B. Barnes, and P. Lipscomb, "Through-focus scanning and scatterfield optical methods for advanced overlay target analysis," Proc. SPIE **7272**, 727214 (2009).
7. V. Vartanian, R. Attota, H. Park, G. Orji, and R. A. Allen, "TSV reveal height and dimension metrology by the TSOM method," Proc. SPIE **8681**, 86812F (2013).
8. A. Arceo, B. Bunday, and R. Attota, "Use of TSOM for sub-11 nm node pattern defect detection and HAR features," Proc. SPIE **8681**, 86812G (2013).
9. S. Usha, P. V. Shashikumar, G. C. Mohankumar, and S. S. Rao, "Through Focus Optical Imaging Technique To Analyze Variations In Nano-Scale Indents," Int. J. Eng. Res. Technol. **2**(5), 97–100 (2013).
10. J.-H. Cho, H.-C. Choi, J.-H. Kang, S.-I. Shin, and H.-B. Kim, "Method of acquiring TSOM image and method of examining semiconductor device," U.S. Patent 20170301079A1 (2017).
11. Y. Qu, J. Hao, and R. Peng, "Machine-learning models for analyzing TSOM images of nanostructures," Opt. Express **27**(23), 33978–33998 (2019).
12. G. Vicidomini, P. Bianchini, and A. Diaspro, "STED super-resolved microscopy," Nat. Methods **15**(3), 173–182 (2018).
13. R. K. Attota and H. Kang, "Parameter optimization for through-focus scanning optical microscopy," Opt. Express **24**(13), 14915–14924 (2016).
14. R. Attota, "Noise analysis for through-focus scanning optical microscopy," Opt. Lett. **41**(4), 745–748 (2016).
15. M. Ryabko, S. Koptyaev, A. Shcherbakov, A. Lantsov, and S. Y. Oh, "Motion-free all optical inspection system for nanoscale topology control," Opt. Express **22**(12), 14958–14963 (2014).
16. M. Ryabko, A. Shchekin, S. Koptyaev, A. Lantsov, A. Medvedev, A. Shcherbakov, and S. Y. Oh, "Through-focus scanning optical microscopy (TSOM) considering optical aberrations: practical implementation," Opt. Express **23**(25), 32215–32221 (2015).
17. R. K. Attota, "Fidelity test for through-focus or volumetric type of optical imaging methods," Opt. Express **26**(15), 19100–19114 (2018).
18. S.-W. Park, G. Park, Y. Kim, J. H. Cho, J. H. Lee, and K. Hwi, "Through-focus scanning optical microscopy with the Fourier modal method," Opt. Express **26**(9), 11649–11657 (2018).
19. R. Peng, J. Jiang, J. Hao, and Y. Qu, "Lateral movement and angular illuminating non-uniformity corrected TSOM image using Fourier transform," Opt. Express **28**(5), 6294–6305 (2020).
20. J. H. Lee, "Through-focus scanning optical microscopy with adaptive optics," SPIE Newsroom, 10–12 (2016).
21. J. H. Lee, J. H. Park, D. Jeong, E. J. Shin, and C. Park, "Tip/tilt-compensated through-focus scanning optical microscopy," Proc. SPIE **10023**, 100230P (2016).
22. J. H. Lee, G. N. Park, J. Jeong, and C. Park, "Through-focus scanning optical microscopy with adaptive optics," Proc. SPIE **10585**, 105850C (2018).
23. S.-W. Park, B. G. You, G. Park, Y. Kim, J. H. Lee, J. H. Cho, Y. Yi, and H. Kim, "Metrological sensitivity improvement of through-focus scanning optical microscopy by controlling illumination coherence," Opt. Express **27**(3), 1981–1990 (2019).
24. S. Stokowski and M. Vaez-Iravani, "Wafer inspection technology challenges for ULSI manufacturing," AIP Conf. Proc. **449**(1), 405–415 (1998).
25. J. M. Beckers, "Adaptive Optics for Astronomy: Principles, Performance, and Applications," Annu. Rev. Astron. Astrophys. **31**(1), 13–62 (1993).
26. V. Marx, "Microscopy: Hello, adaptive optics," Nat. Methods **14**(12), 1133–1136 (2017).
27. R. K. Attota, "Through-focus or volumetric type of optical imaging methods: a review," J. Biomed. Opt. **23**(07), 1 (2018).
28. R. K. Attota and H. Park, "Optical microscope illumination analysis using through-focus scanning optical microscopy," Opt. Lett. **42**(12), 2306–2309 (2017).
29. E. Agocs and R. K. Attota, "Enhancing optical microscopy illumination to enable quantitative imaging," Sci. Rep. **8**(1), 4782 (2018).
30. R. K. Tyson, *Principles of Adaptive Optics* (CRC Press, Taylor and Francis Group, Boca Raton, London, New York, 2015).

Optics EXPRESS

31. P.-Y. Madec, "Overview of deformable mirror technologies for adaptive optics and astronomy," Proc. SPIE **8447**, 844705 (2012).
32. J. H. Lee, T.-K. Uhm, and S.-K. Youn, "First order analysis of thin plate deformable mirrors," J. Korean Phys. Soc. **44**(6), 757–764 (2003).
33. J. H. Lee, Y. C. Lee, and H. J. Cheon, "A circular bimorph deformable mirror for circular/annulus/square laser beam compensation," J. Opt. Soc. Korea **10**(1), 23–27 (2006).
34. R. J. Noll, "Zernike polynomials and atmospheric turbulence," J. Opt. Soc. Am. **66**(3), 207–211 (1976).